

Dynamically generated quadrupole polarization using Floquet adiabatic evolution

G. Camacho , C. Karrasch, and R. Rausch**Technische Universität Braunschweig, Institut für Mathematische Physik, Mendelssohnstrasse 3, 38106 Braunschweig, Germany*

(Received 28 October 2022; revised 1 March 2023; accepted 17 March 2023; published 7 April 2023)

We investigate the nonequilibrium dynamics of the $S = 1$ quantum spin chain subjected to a time-dependent external drive, where the driving frequency is adiabatically decreased as a function of time (Floquet adiabatic evolution). We show that, when driving the rhombic anisotropy term (known as the two-axis countertwisting in the context of squeezed spin states) of a Néel antiferromagnet, we can induce an overall enhancement in the quadrupole polarization, while at the same time suppressing the staggered magnetization order. The system evolves into a new state with a net quadrupole moment and antiferroquadrupolar correlations. This state remains stable at long times once the driving frequency is kept constant. On the other hand, we find that we cannot achieve a quadrupole polarization for the symmetry-protected Haldane phase, which remains robust against such driving.

DOI: [10.1103/PhysRevResearch.5.023015](https://doi.org/10.1103/PhysRevResearch.5.023015)

I. INTRODUCTION

To find quantum states with desired properties, we can look in various spaces: In the chemical space, we can investigate the multitude of natural compounds. This space can be further extended by synthesis, metamaterials, or the replacement of chemical bonds by magneto-optical traps in ultracold quantum gases. Another possibility is to exploit the additional dimension of time and engineer new states in nonequilibrium conditions.

A particularly simple way to create a nonequilibrium state is a quantum quench, where the system is suddenly evolved with a new Hamiltonian. This can be used to observe the melting of equilibrium order parameters, such as string order [1,2], and can lead to quasisteady prethermalized states [3] before heating sets in but does not offer optimal control and is not easily implementable beyond ultracold-atom systems.

Alternatively, one can drive the system out of equilibrium by a periodic external force, e.g., a continuous laser beam with frequency $\Omega = 2\pi/T$ and period T . In practical terms, this setup is well controlled in the high-frequency limit, where one can find the effective Floquet Hamiltonian [4,5] by means of a Magnus expansion of the original Schrödinger equation. In leading order, this results in renormalized system parameters, so that the problem can be analyzed using equilibrium techniques (Floquet engineering). Heating to an infinite-temperature state should take place eventually but is shown to happen on exponentially long time scales for large frequencies, leading to a stable prethermalized state similar to the case of quenches [6,7].

Floquet engineering has been applied very extensively [7–10], and a comprehensive listing of all results is near impossible. For noninteracting systems, the electronic band structure is modified, which becomes interesting if the topological character is changed [11–14]. For interacting systems, a lot of attention has been devoted to the enhancement of superconducting correlations [15–18] (often using intense pulses rather than continuous beams) and the photo-inducement of superconducting orders absent from equilibrium phases, such as η pairing [19–21]. Apart from that, there have been efforts to control the Kondo effect [22], exchange interactions [23], the Dzyaloshinskii-Moriya interaction [24], the magnetization [25], or many-body localization [26].

In equilibrium physics, the concept of adiabaticity is fundamental. In practical terms, it can be used to define and traverse phase diagrams or prepare complex ground states by adiabatically changing the couplings of a Hamiltonian, e.g., using quantum annealing. Extending this concept to Floquet engineering, one can attempt to adiabatically change the drive parameters to further improve the degree of dynamic control of the system [27,28].

In this paper, we adopt the specific protocol of initiating the system by driving a term with $\Omega = \infty$, followed by an adiabatic decrease of Ω [29,30]. This adiabatically propagated state is called the *Floquet ground state* [30], and Ω is freed up as an additional control parameter in the procedure. This has been first studied for the integrable transverse-field Ising model, in which case the state was seen to undergo topological phase transitions and Kibble-Zurek scaling was observed [29,30].

Fortunately, in the case of one-dimensional (1D) chains, this adiabatic Floquet protocol lends itself to an efficient simulation even for nonintegrable systems using matrix-product states (MPSs). The initial state is guaranteed to have low entanglement for the class of gapped chains in accordance with the area law. This is a key property that is exploited by the MPS formalism [31]. Furthermore, if the change of frequency

*r.rausch@tu-braunschweig.de

is slow enough, the entanglement is expected to only grow slowly, and long propagation times may be reached. This stands in contrast to quench dynamics, where the entanglement entropy increases linearly with time [32], while the MPS bond dimension (i.e., the number of variational parameters to represent the state) must increase exponentially.

In this paper, we show that the adiabatic Floquet protocol can be used to convert a conventional Néel antiferromagnetic (AFM) state into an unconventional antiferroquadrupolar (AFQ) state. More specifically, we apply the protocol to the nonintegrable $S = 1$ spin chain, a system which is mainly interesting for its symmetry-protected topological Haldane phase and the potential for spin-nematic (quadrupolar) order. The latter is a state with nonvanishing anisotropic second-order expectation values of the type $\langle S_j^\alpha S_j^\beta \rangle \neq 0$, while having a vanishing first-order expectation $\langle S_j^\alpha \rangle = 0$ (where $S_j^{\alpha=x,y,z}$ is a spin operator). Thus, it is an interesting quantum state that carries no magnetic moment but still breaks the spin-rotational symmetry via a more complicated order parameter. A spin nematic can be regarded as something between a ferromagnet and a spin liquid: While it lacks magnetic order like the latter, it still breaks the rotational symmetry like the former and has a preferred axis. The name derives from the physics of nematic liquid crystals, which in a similar sense constitute a phase between a liquid and a solid [33]. While quadrupolar order is in principle possible in the $S = 1$ chain, in the following section, we discuss that it is not easily achievable in equilibrium, motivating an extension to driven systems.

Starting from the ground state of an initial Hamiltonian with $\Omega = \infty$, we slowly drive the system from the high-frequency to the midfrequency region, representing the wave function as a MPS. We find that, if the initial state is in the symmetry-protected Haldane phase, it still remains remarkably robust against the drive, and no new phase transition is found. On the other hand, if the initial state is in a trivial ordered phase, then we can induce an overall quadrupolar moment and enhanced correlations, eventually reaching a stable phase with long-range AFQ order, where the staggered magnetization is suppressed.

II. MODEL

A. Initial Hamiltonians

We consider a 1D chain of localized spins with $S = 1$ at zero temperature. The real system under consideration might in fact be a two-dimensional (2D) or three-dimensional array of such chains, where the interchain coupling is captured on the mean-field level by a staggered magnetic field h [34–37]. Experimentally, such systems are realized in various Ni- and V-based compounds [38–56] (see also Fig. 1).

The Hamiltonian is an extended variant of the Heisenberg spin chain:

$$H_{\text{Heis}} = J \sum_j \vec{S}_j \cdot \vec{S}_{j+1} + D \sum_j (S_j^z)^2 - h \sum_j (-1)^j S_j^z, \quad (1)$$

where J is the exchange interaction parameter, and $\vec{S}_j = (S_j^x, S_j^y, S_j^z)$ represents the spin-1 operator at the j th site, with $S_j^{\alpha=x,y,z}$ representing the different spin projections. As the local basis $|\sigma\rangle$, we take the eigenbasis of S_j^z and denote the

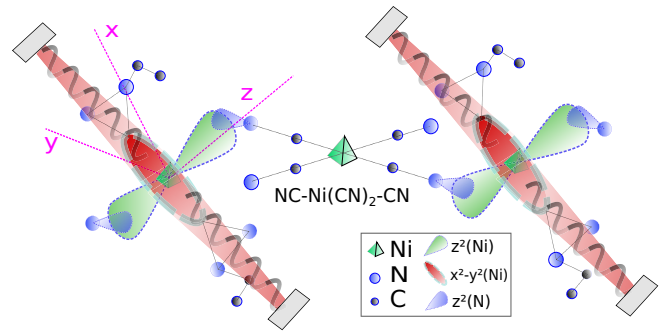


FIG. 1. The compound $\text{Ni}(\text{C}_2\text{H}_8\text{N}_2)_2\text{Ni}(\text{CN})_4$ (NENC) under the action of a periodic driving in the x^2-y^2 orbital of the Ni(II) atoms. The figure is inspired by fig. 1 in Ref. [57], but we have added a possible experimental driving setup. The structure of the chain repeats in the horizontal direction. Molecular orbitals from the Ni and N atoms have been represented in the x, y, z geometry by the lobes (see legend). Each Ni(II) is attached to the next one by a $\text{NC-Ni}(\text{CN})_2\text{-CN}$ configuration. The magnetic properties of such Ni compounds have been studied experimentally. A theoretical description of these compounds is proposed by effective Hamiltonians in the form of Eq. (1) representing the $S = 1$ chain of the Ni(II). The experimental realization sketched in this figure corresponds to the driving protocol given by Eq. (12) of this paper, where the drive in the xy plane (represented as a sinusoidal wave) continuously changes the probability distribution of electronic x^2-y^2 orbital in the Ni(II) atoms.

eigenvectors as $|\sigma\rangle = |+\rangle, |0\rangle, |-\rangle$ with the eigenvalues of $+1, 0$, and -1 , respectively. Finally, h is the staggered magnetic field, while D is the anisotropy in the z direction (easy axis for $D < 0$ and easy plane for $D > 0$). We set $\hbar = 1$ and $J = 1$, thereby measuring all energies in units of J and times in units of \hbar/J .

For $D = h = 0$, there exists a gapped phase (the Haldane phase), which (for periodic boundary conditions) has a unique symmetry-protected ground state with exponentially decreasing spin-spin correlations. The robustness of the Haldane phase has been a focal point of previous studies in equilibrium [58–64], where it was found that it can be characterized by a nonlocal string order parameter [65–67]:

$$O_{\text{string}}^{\alpha=x,y,z} = \lim_{|j-k| \rightarrow \infty} \left\langle S_j^\alpha \exp \left(i\pi \sum_{l=j+1}^{k-1} S_l^\alpha \right) S_k^\alpha \right\rangle, \quad (2)$$

and by a global twofold degeneracy in the entanglement spectrum. It is protected by a combination of inversion symmetry, time-reversal (in the sense $S^{x,y,z} \rightarrow -S^{x,y,z}$) and combined rotations of π about a pair of axes [63]. Since a finite h breaks all these symmetries at once, even a small value destroys the Haldane phase [35]. However, it remains robust against the anisotropy term, which does not break any of the above symmetries [62–64]. In this case, the Haldane phase is a thermodynamic phase, which is stable in an extended region of the phase diagram, eventually losing in competition to strong- D phases (see below) once D exceeds a critical value. An interesting question is thus how this robustness extends into nonequilibrium.

The other limiting cases of Eq. (1) are as follows: For $D \rightarrow +\infty$, the ground state is given by a product state of local $|0\rangle$ projections. In the $D \rightarrow -\infty$ limit, the ground state is twofold degenerate, given by the Néel state $\dots |+\rangle |-\rangle |+\rangle |-\rangle \dots$ and the Néel state shifted by one lattice site: $\dots |-\rangle |+\rangle |-\rangle |+\rangle \dots$. For $h \rightarrow \pm\infty$, the ground state is given by a unique Néel state.

The $S = 1$ chain is also arguably the simplest system that allows for quadrupolar exchange. The quadrupole operator is defined as the traceless tensor:

$$Q_j^{\alpha\beta} = S_j^\alpha S_j^\beta + S_j^\beta S_j^\alpha - \frac{2}{3}S(S+1)\delta_{\alpha\beta}. \quad (3)$$

It has five linearly independent components that can be grouped into a vector:

$$\vec{Q}_j = \begin{pmatrix} Q_j^{x^2-y^2} \\ Q_j^{3z^2-r^2} \\ Q_j^{xy} \\ Q_j^{yz} \\ Q_j^{xz} \end{pmatrix} = \begin{pmatrix} (S_j^x)^2 - (S_j^y)^2 \\ \frac{1}{\sqrt{3}}[3(S_j^z)^2 - S(S+1)] \\ S_j^x S_j^y + S_j^y S_j^x \\ S_j^y S_j^z + S_j^z S_j^y \\ S_j^x S_j^z + S_j^z S_j^x \end{pmatrix}, \quad (4)$$

so that $\sum_{\alpha\beta} Q_j^{\alpha\beta} Q_j^{\alpha\beta} = 2\vec{Q}_j \cdot \vec{Q}_j$. Quadrupolar exchange thus requires a product of four spin operators and is usually discussed within the bilinear-biquadratic model [68,69], given by

$$H_{\text{blbq}} = J \sum_j \vec{S}_j \cdot \vec{S}_{j+1} + J_q \sum_j (\vec{S}_j \cdot \vec{S}_{j+1})^2. \quad (5)$$

Because of the identity:

$$\vec{Q}_i \cdot \vec{Q}_j = 2(\vec{S}_i \cdot \vec{S}_j)^2 + \vec{S}_i \cdot \vec{S}_j - \frac{2}{3}[S(S+1)]^2, \quad (6)$$

the Hamiltonian in Eq. (5) boils down to a competition of ordinary exchange interaction and quadrupolar exchange. In 1D, quantum fluctuations generally prevent spontaneous ordering unless the order parameter is conserved. In this case, a quadrupolar state may rather be defined via quadrupolar correlations that dominate over spin-spin correlations. Such correlations are found with a three-site period for $J, J_q > 0$ and $J_q/J > 1$ [70]. For $J < 0$, a ferroquadrupolar order was initially predicted close to the ferromagnetic phase [71], but highly accurate MPS calculations demonstrate that it either does not exist (with a dimerized phase found instead) or only exists in a very narrow parameter regime [70,72]. In 2D, quadrupolar phases are better defined, and a finite quadrupole moment generally arises for $|J_q|/|J| > 1$ [73,74].

We note that the choice:

$$H_{\text{AKLT}} = \sum_j \vec{S}_j \cdot \vec{S}_{j+1} + \frac{1}{3} \sum_j (\vec{S}_j \cdot \vec{S}_{j+1})^2, \quad (7)$$

yields the famous Affleck-Kennedy-Lieb-Tasaki (AKLT) ground state [60,61], which belongs to the Haldane phase, but is exactly representable by an MPS with very low entanglement. From a technical point of view, it is thus a more convenient representative member of the Haldane phase than Eq. (1) with $h = D = 0$.

A possibility to generate finite quadrupolar moments in 1D is the explicit breaking of the spin-SU(2) symmetry via the

so-called *rhombic single-ion anisotropy* [75–77]:

$$\begin{aligned} \delta H_E &= E \sum_j [(S_j^x)^2 - (S_j^y)^2] \\ &= E \sum_j Q_j^{x^2-y^2} = \frac{E}{2} \sum_j [(S_j^+)^2 + (S_j^-)^2], \end{aligned} \quad (8)$$

where we have introduced the standard spin-flip operators $S_j^\pm = S_j^x \pm iS_j^y$. A more general coupling to the square of the spin operator is also possible [77,78]. In the context of squeezed spin states, the term in Eq. (8) is known as the *two-axis countertwisting* (TACT) [79], and there are several proposals of how to implement it [80]. In equilibrium, a strong value of E will induce a finite quadrupole moment in the direction of $(Q^{x^2-y^2})$, similar to how an external field induces a finite magnetization [75]. However, this requires finding a material with large E and small D at the same time.

Recently, attention has shifted to a different regime, where bond-nematic rather than local order might be found. For an $S = \frac{1}{2}$ system in a strong magnetic field close to saturation, deviations in magnetization are given by magnons. If the effective interaction between these magnons is attractive, they may form pairs and condense, with nonzero quadrupolar correlations $\langle S_i^+ S_j^+ \rangle$ playing the same role as anomalous expectation values of fermion-pair creation operators $\langle c_i^\dagger c_j^\dagger \rangle$ in a superconductor [81]. The best-documented experimental example where this may occur is LiCuVO₄ [82,83]. The corresponding experiments are quite challenging and need to be performed in magnetic fields of 45–50 T.

Summarizing, a spin-nematic state is an exotic nonmagnetic state with a higher-level order parameter. The minimal spin value to observe it locally is $S = 1$. A stabilization of this state requires strong biquadratic exchange or a strong anisotropy. However, both are expected to be weak in real materials or require finding a fine-tuned point [84–86], so that the part of the phase diagram where spin-nematic phases are predicted could not be explored in practice. Attention has therefore shifted to the different physical regime of magnon pairing in high magnetic fields for $S = \frac{1}{2}$ materials, which has its own challenges. Here, we pursue an alternative idea, namely, the purposeful enhancement of quadrupolar interactions using nonequilibrium driving, starting from an ordinary $S = 1$ system (Haldane chain or Néel antiferromagnet).

B. Floquet adiabatic protocol

We evolve a system in the presence of a time-dependent term $Af[t, \Omega(t)]V$:

$$H(t) = H_0 + Af[t, \Omega(t)]V, \quad (9)$$

where H_0 is the unperturbed Hamiltonian, $f[t, \Omega(t)]$ is the periodic envelope function of the drive, $\Omega(t)$ is the drive frequency, A is its amplitude, and V is the operator of the drive.

It is convenient to choose an envelope function that averages to zero over one cycle:

$$\frac{1}{T} \int_0^T d\tau f(\tau, \Omega) = 0. \quad (10)$$

Specifically, we set

$$f[t, \Omega(t)] = \sin[\Omega(t)t]. \quad (11)$$

This means that, for $\Omega(t=0) = \infty$, the state at $t=0$ can be obtained as the ground state of H_0 and is a legitimate Floquet state.

To observe quadrupolar order in our setup, we choose to drive the rhombic anisotropy Eq. (8), which is quadratic in the spin operators (cf. Fig. 1):

$$Af[t, \Omega(t)]V = Af[t, \Omega(t)] \sum_j [(S_j^x)^2 - (S_j^y)^2]. \quad (12)$$

For $t > 0$, we start with a frequency of Ω_0 that is large enough to be connected with the infinite-frequency state at $t=0$. We then adiabatically decrease the frequency in the range $\Omega(t) \in [\Omega_f, \Omega_0]$ ($\Omega_0 > \Omega_f$) on a time window of length t_f (see Appendix A for more details). After that, we assess whether a steady state has been reached by evolving the state with constant Ω_f for another multiple of t_f , i.e., until the end time $t_{\text{end}} = \alpha t_f$, where $\alpha > 1$ is a scaling factor. In other words, the steady state is observed on a time scale of $(\alpha - 1)t_f$.

The meaning of these control parameters is as follows: (1) The target time t_f controls adiabaticity, whereby larger values make the process more adiabatic, so that we would like to choose t_f as large as possible. (2) For the final frequency Ω_f , the most interesting regime is on the energy scale of the system or below it, i.e., $O(10^0) - O(10^{-1})$ in units of J . However, if Ω becomes so small that $\Omega^{-1} \sim t_f$, the system cannot be considered locally periodic at any time, and the Floquet theorem loses its validity. Therefore, one should choose a range of Ω for which all values satisfy $\Omega t_f \gg 2\pi \forall \Omega \in [\Omega_f, \Omega_0]$ [29], which means that smaller Ω_f must be offset by larger t_f .

Considering all these tradeoffs, we set $\Omega_0 = 100.0$, $\Omega_f \geq 10.0$, $t_f = 62.82$, and $\alpha = 1.5, 2.5$.

III. METHODS

A. Time-evolving block decimation

We use the infinite time-evolving block decimation (iTEBD) with a fourth-order Suzuki-Trotter decomposition [31,87] to compute time evolution of a given MPS directly in the thermodynamic limit. The main control parameter is the bond dimension χ , which encodes the amount of entanglement.

The MPS $|\psi\rangle$ has a unit cell of $L_{\text{cell}} = 2$ for a finite staggered field in Eq. (1). We represent it in the standard Γ - Λ notation [88]:

$$|\psi\rangle = \sum_{\{\sigma_i\}} \dots \Gamma^{A\sigma_i} \Lambda^{AB} \Gamma^{B\sigma_{i+1}} \Lambda^{BA} \dots |\dots \sigma_i \sigma_{i+1} \dots\rangle, \quad (13)$$

with A and B denoting the sublattices, and $\sigma_i = \{+, 0, -\}$. The AKLT state (Sec. IV A) can be expressed analytically as a MPS with a bond dimension of $\chi = 2$. The Néel ground state (Sec. IV B) is computed from an imaginary time evolution with a fixed bond dimension of $\chi = 200$ and a decreasing Trotter step size until convergence has been reached; we have checked that using $\chi = 120$ or $L_{\text{cell}} = 4, 6$ does not change the results and also cross-checked with the Variational

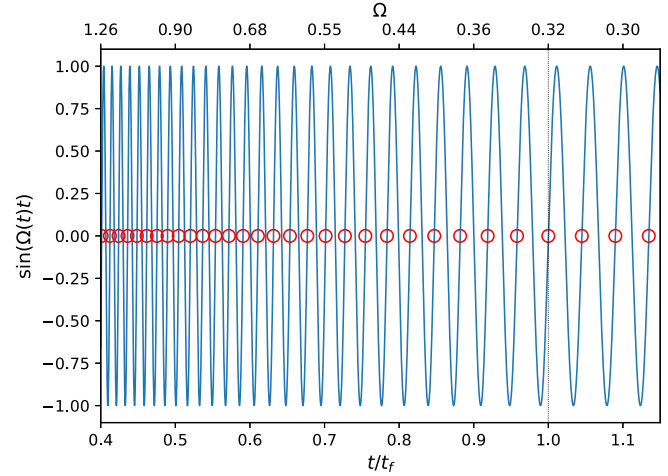


FIG. 2. The drive envelope function $f(t)$, Eq. (11), with $\Omega_f = 0.3$. We use an *intermittent* measurement process, where the red circles correspond to the measurement times of the observables. On the top axis, we have represented the corresponding values of the driving frequency Ω , which is kept constant at $\Omega = \Omega_f$ for $t/t_f > 1$.

Uniform MPS (VUMPS) algorithm [89] as an independent benchmark.

During the real-time evolution, it is convenient to choose a variable Trotter step size Δt that depends on the current period. We do not let it exceed the maximum value of $\Delta t = 0.01$. Furthermore, we set an initially fixed bond dimension of $\chi = 200$ (for the quench starting from the AKLT state, the initial bond dimension $\chi = 2$ is increased such that the state is encoded exactly until $\chi = 200$ is reached). This is sufficient for an upper bound of the discarded weight (defined as the sum of discarded weights on each Trotter substep) of $\epsilon = 10^{-5}$. In other words, fixing $\epsilon = 10^{-5}$ does not lead to an increase of the bond dimension beyond $\chi = 200$, which seems reasonable due to the adiabatic nature of the quench. Further comments on this issue as well as a comparison with exact diagonalization (ED) data can be found in Appendix B.

B. Measurement events and the steady-state limit

When we keep track of all observables in a continuous fashion, the micromotion of the Hamiltonian dynamics leads to the appearance of oscillations as a consequence of the drive given by Eq. (11). We ignore this micromotion by an intermittent measuring at some of the zeros of the drive, as indicated in Fig. 2. This subset of N measuring points is defined by

$$t^* = \{t_j^*\} \subset [0, \alpha t_f] \mid f(t_j^*) = 0, \quad \forall j = 1, \dots, N. \quad (14)$$

Furthermore, we define the steady-state limit (SSL) value of an observable O in the Heisenberg picture by averaging over the last N_{SSL} measurement times:

$$\langle O \rangle_{\text{SSL}} = \frac{\sum_{k=1}^{N_{\text{SSL}}} \langle O(t_k^*) \rangle}{N_{\text{SSL}}}, \quad t_k^* > 2t_f. \quad (15)$$

Due to computational limitations, the above definition is strictly speaking a quasisteady state, in the sense that the

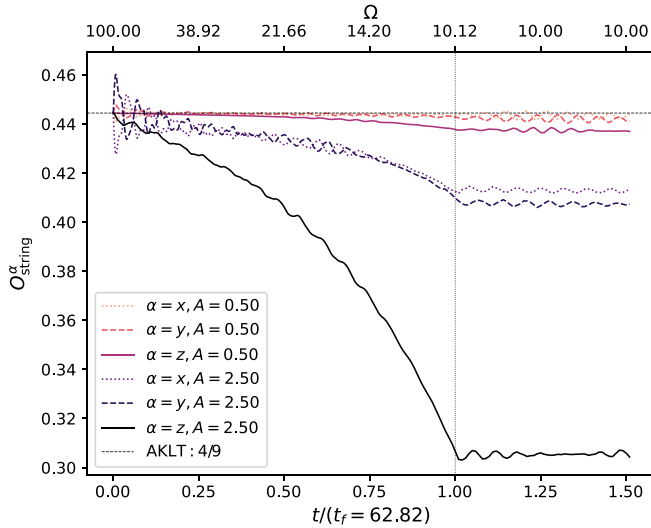


FIG. 3. Time evolution of the string order parameter Eq. (2) in the x, y, z directions during the drive starting from the Haldane phase (see Sec. IV A) for $\Omega_f = 10.0$, $A = 0.5, 2.5$. The drive fails to suppress the string order, with the transverse z direction being the most affected. The initial AKLT value of $\frac{4}{9}$ is marked by the horizontal dashed line. The Haldane phase is therefore robust against the drive Eq. (12).

reachable times are finite but long on the intrinsic time scale: $\alpha t_f \gg \hbar/J = 1$ ($\alpha = 1.5, 2.5$).

IV. RESULTS

A. Driving from the Haldane phase

We apply the protocol given by Eqs. (9) and (12) to the AKLT state, which is the ground state of the Hamiltonian Eq. (7) ($H_0 = H_{\text{AKLT}}$) and an ideal representative of the Haldane phase.

Since the drive does not break the protective symmetries of the Haldane phase, we expect the phase to be robust at least against small amplitudes. Numerically, we can go up to $A = 2.5$ and find that the drive is still unable to destroy the Haldane phase because it cannot destroy the string order. For the initial AKLT state, the string order is isotropic with a value of $O_{\text{string}}^{\alpha=x,y,z} = \frac{4}{9}$. Figure 3 shows its evolution, and we find that it remains finite in all directions. (Note that this stands in contrast with a sudden quench, which can destroy the order [1,2].) Furthermore, we find no noticeable increase of a quadrupole polarization or correlations (not shown).

Our conclusion is that the robustness of the Haldane phase is difficult to overcome in our setup, and one needs to start from an initial ground state which should already incorporate the breaking of its protective symmetries. To this end, we explore the driving protocol of Eq. (12) and apply it to the initial Hamiltonian given by Eq. (1) with nonzero h and D .

B. Driving from a trivial phase

1. Choice of parameters

Relatively small anisotropies and interchain couplings are enough to induce an ordered phase for the $S = 1$ chain. Still,

in a lot of Ni-based compounds, both are weak enough to keep them in the Haldane phase or at the edge of the phase transition line [36]. An exception is CsNiCl_3 , which shows Néel order below a critical temperature, and for which $h = 0.051$, $D = -0.038$ have been deduced [34,39] (though not without uncertainty [38]). A very large anisotropy of $D \sim -1.5$ was recently proposed for $\text{BaMo}(\text{PO}_4)_2$ [90].

To demonstrate the general principle, we set $H_0 = H_{\text{Heis}}$ [Eq. (1)], $D = -0.2$, and $h = +0.1$, which puts the initial system firmly into the ordered Néel phase: The ground state has a finite staggered spin polarization of $(-1)^j \langle S_j^z \rangle \approx 0.74$ in the z direction. Spin-spin correlations of the z projection show AFM long-range order, while quadrupolar correlations are short ranged [see Fig. 4(b) for $t = 0$].

2. Suppression of AFM Néel order and emergence of quadrupole polarization

The time evolution of the staggered magnetization $(-1)^j \langle S_j^z \rangle$ and the quadrupole component $(-1)^j \langle Q_j^{xy} \rangle$ are presented in Fig. 5. The initial staggered magnetization of the Néel state is always reduced by the drive and is completely suppressed for $A \approx 8$. This coincides with the emergence of a staggered net quadrupole moment in the Q^{xy} direction, which becomes finite and survives in the SSL, where $\Omega_f = 10.0$ is kept constant. There is an optimal value of A where the quadrupole polarization is highest, i.e., it tends to be smaller for both very small and very large A .

We note that the polarization is obtained in the third component Q^{xy} of the quadrupolar operator Eq. (4), while the driving term only couples to the first component $Q^{x^2-y^2}$. This axial enhancement is somewhat analogous to the behavior observed in Ref. [25], where switching on a rotating magnetic field in the xy plane induces a finite polarization of the z component of the spin, i.e., perpendicular to the plane of the driving.

3. The AFQ correlations

The above result suggests the dynamical emergence of a spin-nematic state due to application of the drive, where the quadrupole polarization dominates over the magnetization. To further investigate this state, we fix $A = 6.0$ and show the quadrupole correlations $\langle Q_j^{xy} Q_{j+r}^{xy} \rangle$ in Fig. 4. The appearance of an AFQ state is characterized by negative (positive) correlations at odd (even) sites r that remain stable for times $t/t_f > 1$ in the SSL. Note that there is a sign switch as a function of time for $r = 1$. In Fig. 4(b), we show the profile of the quadrupole correlation characteristic of the AFQ state in the SSL compared with their initial values at $t = 0$.

We point out that our resulting state is distinct from the large- E phases reported in Ref. [75], where the polarization is in the direction of $Q^{x^2-y^2}$, i.e., along the applied field E . If the ground state can be chosen to be real valued, then $\langle Q_j^{xy} \rangle = 0$ must necessarily hold in equilibrium. A polarization in the direction of Q^{xy} therefore results from the time propagation during the drive, which gives an imaginary part to the wave function. Thus, our resulting state generally has no equilibrium analog for systems described by Eqs. (1) and (5), even if the rhombic anisotropy term in Eq. (8) is also present, unless spontaneous breaking of time-reversal symmetry results in a

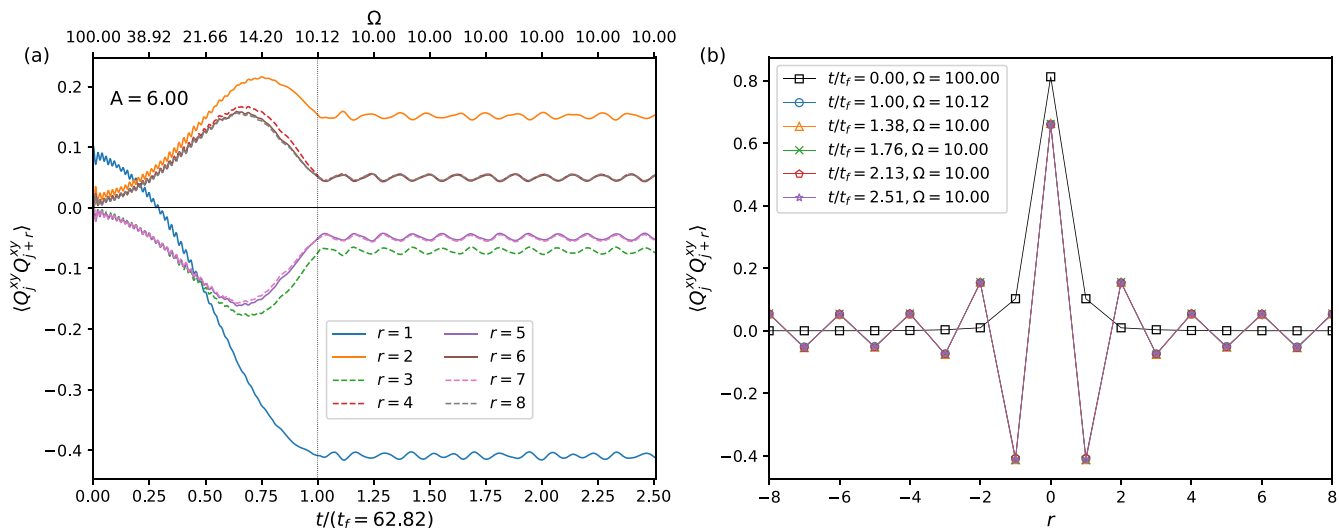


FIG. 4. (a) Time evolution for the quadrupole correlations $\langle Q_j^{xy} Q_{j+r}^{xy} \rangle$ [see Eq. (4)] for the setup as in Fig. 5 and an amplitude of the drive $A = 6.0$ [Eq. (12)]. We observe the development of an antiferroquadrupolar (AFQ) state, in which odd (even) values of r become negative (positive). (b) The corresponding AFQ profile measured at specific time points $t/t_f \geq 1$, compared with the initial value at $t = 0$; straight lines between data points are included as a guide to the eye. The overlap of profiles at constant $\Omega = \Omega_f$ for times $t/t_f \geq 1$ indicates the survival of the AFQ state in the steady-state limit.

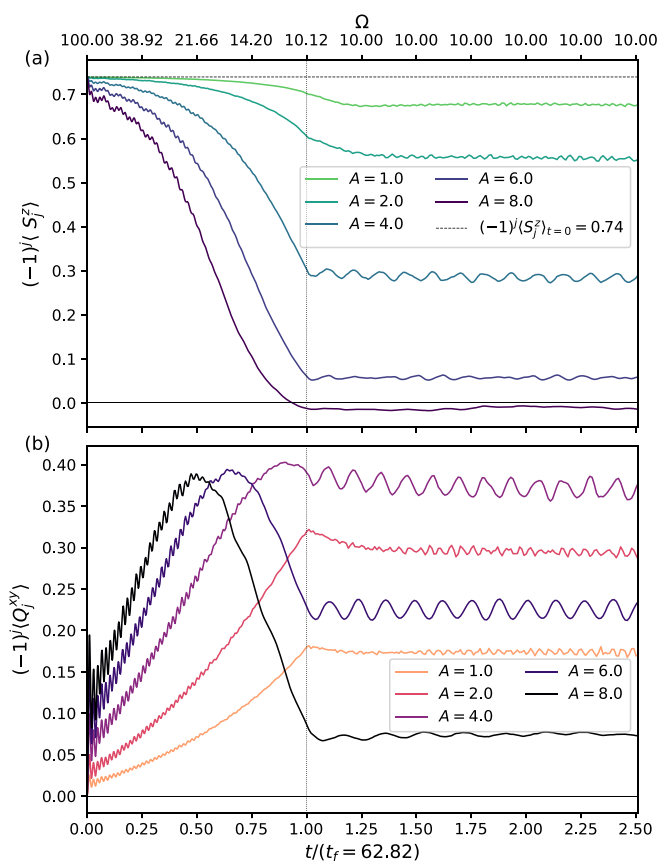


FIG. 5. Time evolution after a quench starting from the trivial Néel phase ($\Omega_f = 10$) of (a) the staggered magnetization $(-1)^j \langle S_j^z \rangle$, decaying as a function of time for strong values of the drive amplitude A [Eq. (12)], and (b) the net quadrupole moment $|(-1)^j \langle Q_j^{xy} \rangle| \neq 0$ [see Eq. (4)] induced by the drive. Both observables remain steady for times $t > t_f$.

complex-valued ground state. We discuss this in some more detail in Sec. IV B 5.

4. Phase diagram in the SSL

To better characterize the dynamically obtained AFQ state and explore its stability at longer times, we study the phase diagram in the SSL for the two order parameters of the staggered magnetization $(-1)^j \langle S_j^z \rangle$ and the quadrupole polarization $(-1)^j \langle Q_j^{xy} \rangle$, as a function of the target frequencies and driving amplitudes (Ω_f, A). The spin-nematic regime is reached when $(-1)^j \langle S_j^z \rangle_{\text{SSL}} \approx 0$ and $(-1)^j \langle Q_j^{xy} \rangle_{\text{SSL}} \neq 0$ for an average over the steady-state regime Eq. (15). We define the crossover parameter between the two regimes as

$$r_{\text{SSL}} = \arctan \left(\left| \frac{\langle Q_j^{xy} \rangle_{\text{SSL}}}{\langle S_j^z \rangle_{\text{SSL}}} \right| \right) \in \left[0, \frac{\pi}{2} \right]. \quad (16)$$

Figure 6(a) shows the phase diagram for r_{SSL} . We distinguish three well-differentiated regions: There is a magnetized region $r_{\text{SSL}} \approx 0$, where the staggered magnetization dominates, as in the initial ground state. The black dashed line is an orientative contour line for $r_{\text{SSL}} = \pi/4$, which separates the magnetized region from a region where the two polarizations are of approximately equal strength, which we call the *hybrid* region. Finally, the straight lines delineate the spin-nematic region $r_{\text{SSL}} \approx \pi/2$, where $\langle S_j^z \rangle \rightarrow 0$.

The effect of reducing the target frequency Ω_f on both the staggered magnetization and the quadrupolar moment is shown in Figs. 6(b) and 6(c). In the small- A region, the systematics of the AFM order and AFQ order are opposite, so that decreasing the frequency leads to weaker AFM polarization and stronger AFQ polarization. In the large- A region, the systematics is the same, and decreasing the frequency leads to a weakening in both.

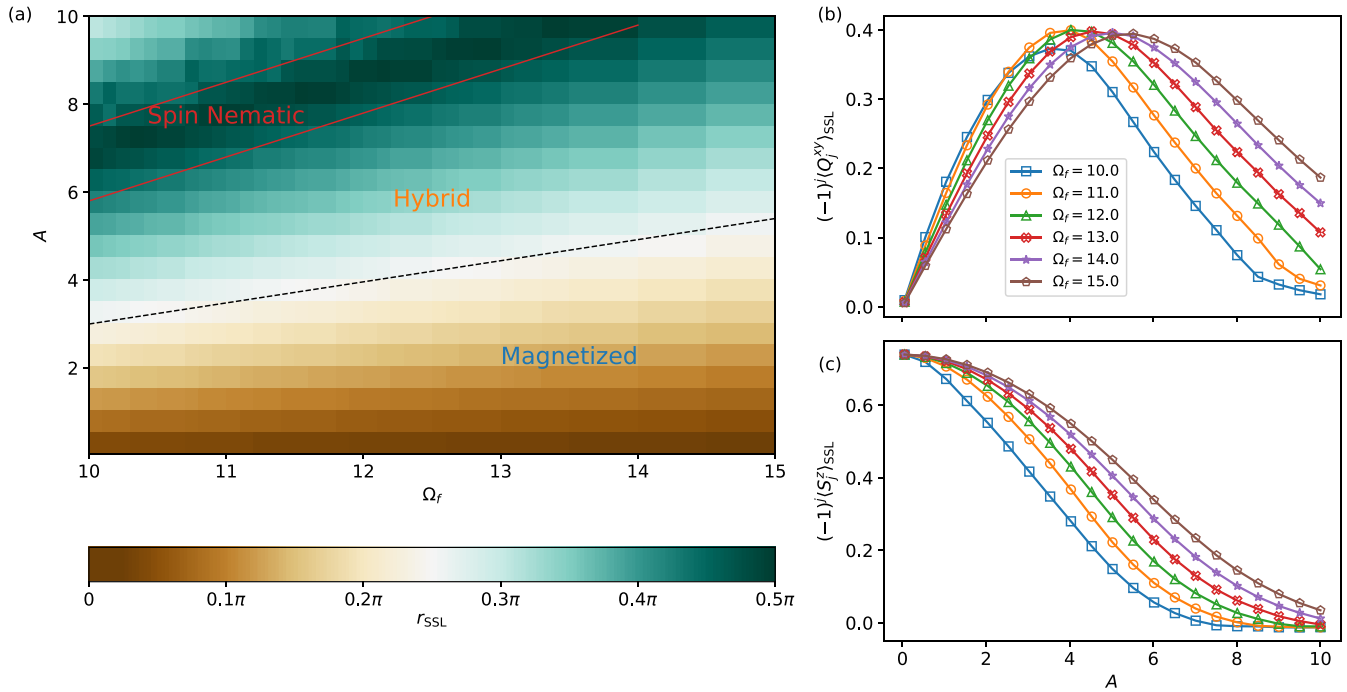


FIG. 6. (a) Phase diagram in the steady-state limit (SSL) following a quench from the trivial Néel phase for the crossover parameter r_{SSL} defined in Eq. (16). The three regimes are (1) magnetized: $r_{\text{SSL}} < \pi/4$, (2) hybrid: $r_{\text{SSL}} \gtrsim \pi/4$, and (3) spin-nematic: $r_{\text{SSL}} \approx \pi/2$. (b) The SSL values of the emerging quadrupole moment for different Ω_f as a function of the driving amplitude A . Reaching smaller Ω_f enhances the net quadrupole moment requiring smaller amplitudes A . Strong values of A tend to suppress the overall enhancement of the quadrupole moment, cf. Fig. 5. (c) The SSL value for the staggered magnetization at different Ω_f as a function of the driving amplitude A . A smaller Ω_f requires smaller A to suppress the Néel order. Straight lines between data points in (b) and (c) are a guide to the eye.

5. The AFQ wave function

Despite the apparent simplicity of the final xy -AFQ state, we find that it is entangled and cannot be written down as a simple analytical wave function. However, we can heuristically attempt to write it down as a simplified MPS by restricting ourselves to the three largest eigenvalues of the entanglement spectrum Λ^{AB} and Λ^{BA} (for the sublattices A and B) in Eq. (13).

Analyzing the numerical result for the ground state, we find that it approximately has the following MPS structure:

$$\Gamma^{\text{A},+} = \begin{pmatrix} -a_{11}^+ & 0 & 0 \\ 0 & 0 & 0 \\ 0 & 0 & 0 \end{pmatrix}, \quad (17)$$

$$\Gamma^{\text{A},0} = \begin{pmatrix} 0 & a_{12}^0 & 0 \\ -a_{12}^0 & 0 & 0 \\ 0 & 0 & 0 \end{pmatrix}, \quad (18)$$

$$\Gamma^{\text{A},-} = \begin{pmatrix} 0 & 0 & -a_{13}^- \\ 0 & a_{22}^- & 0 \\ a_{13}^- & 0 & 0 \end{pmatrix}, \quad (19)$$

$$\Gamma^{\text{B},+} = -\Gamma^{\text{A},-} \quad (20)$$

$$\Gamma^{\text{B},0} = -\Gamma^{\text{A},0}, \quad (21)$$

$$\Gamma^{\text{B},-} = -\Gamma^{\text{A},+}, \quad (22)$$

where $a_{ij}^\sigma = (\Gamma^{\text{A},\sigma})_{ij}$ denotes the nonzero matrix entries.

After switching on the drive, we keep monitoring the pattern of nonzero entries and find that the xy -AFQ state shows the following structure:

$$\Gamma^{\text{A},+}[a_{ij}^+(t)] \approx \begin{bmatrix} a_{11}^+(t) & 0 & a_{13}^+(t) \\ 0 & a_{22}^+(t) & 0 \\ a_{31}^+(t) & 0 & a_{33}^+(t) \end{bmatrix}, \quad (23)$$

$$\Gamma^{\text{A},0}[a_{ij}^0(t)] \approx \begin{bmatrix} 0 & a_{12}^0(t) & 0 \\ a_{21}^0(t) & 0 & a_{23}^0(t) \\ 0 & a_{32}^0(t) & a_{33}^0(t) \end{bmatrix}, \quad (24)$$

$$\Gamma^{\text{A},-}[a_{ij}^-(t)] \approx \begin{bmatrix} a_{11}^-(t) & 0 & a_{13}^-(t) \\ 0 & a_{22}^-(t) & 0 \\ a_{31}^-(t) & 0 & a_{33}^-(t) \end{bmatrix}, \quad (25)$$

$$\Gamma^{\text{B},\sigma}(t) = \Gamma^{\text{A},\sigma}[a_{ij}^\sigma(t) \rightarrow b_{ij}^\sigma(t)], \quad \sigma \in \{+, 0, -\}, \quad (26)$$

$$\Lambda^{\text{AB}}(t) = \text{diag}[\Lambda_0^{\text{AB}}(t), \Lambda_1^{\text{AB}}(t), \Lambda_2^{\text{AB}}(t)], \quad (27)$$

$$\Lambda^{\text{BA}}(t) = \Lambda^{\text{AB}}(t). \quad (28)$$

Moreover, we also observe:

$$|a_{ij}^\pm(t)| \approx |b_{ij}^\mp(t)|, \quad |a_{ij}^0(t)| \approx |b_{ij}^0(t)|. \quad (29)$$

As a technical detail, note that the reduced MPS also needs to be renormalized.

Figure 7 compares $\langle Q_{s=\text{A,B}}^{\text{xy}} \rangle$ obtained with the full and with the heuristically reduced wave function, with overall good

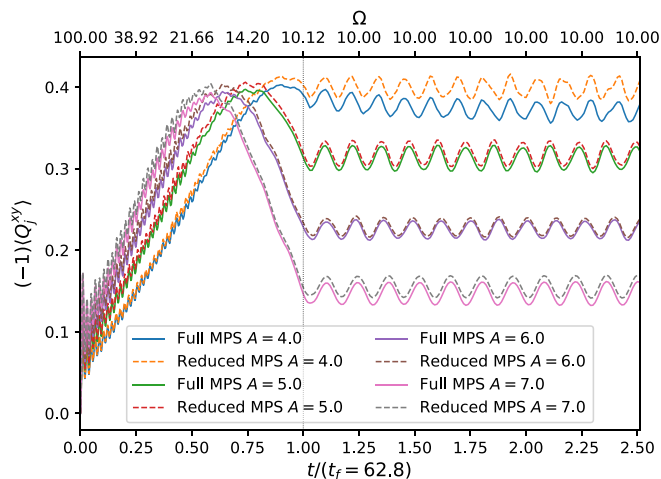


FIG. 7. Comparison between the net quadrupole moment [Eq. (4)] in the Q^{xy} direction obtained from the full matrix-product states (MPS) and the reduced MPS obtained by truncating to the three dominant eigenvalues of the reduced density matrix (see Sec. IV B 5). The qualitative behavior is reliably captured by the smaller MPS.

agreement. To derive an analytic expression for $\langle Q_{s=A,B}^{xy} \rangle$, we note that Q_s^{xy} can be written using $Q_s^\pm = (S_s^\pm)^2$, $S_s^\pm = S_s^x \pm iS_s^y$ as follows:

$$Q_s^{xy} = \frac{i}{2}(Q_s^- - Q_s^+), \quad (30)$$

$$\langle Q_s^{xy} \rangle = \frac{\text{Im}(\langle Q_s^+ \rangle - \langle Q_s^- \rangle)}{2}. \quad (31)$$

We find

$$\langle Q_s^\pm \rangle = \frac{1}{2} \sum_{i,j} [\Lambda_i^{AB} \Lambda_j^{BA}]^2 (\Gamma_{ji}^{s,\pm})^* \Gamma_{ij}^{s,\mp}. \quad (32)$$

Equation (32) shows that, for the initial MPS in Eq. (17), $\langle Q_s^\pm \rangle = 0$, as the matrices $\Gamma^{s,\pm}$ do not share common matrix elements at equal row and column indices. Conversely, the driven state given by Eq. (23) contains nonzero products between the matrix elements and yields a net quadrupole moment $\langle Q_j^{xy} \rangle$.

Furthermore, we see that any contribution to $\langle Q_s^{xy} \rangle$ must come from the imaginary part of $\langle Q_s^\pm \rangle$. This implies that the matrix elements of $\Gamma^{s,\pm}$ must contain imaginary parts, which are acquired in the course of the unitary time evolution (beyond a trivial global phase). This shows that the obtained xy -AFQ state cannot be engineered from an equilibrium configuration by means of an arbitrary variation of the parameters of the model, provided that time-reversal symmetry holds (i.e., the ground-state wave function can be chosen real valued).

V. SUMMARY

We have demonstrated that it is possible to convert a conventional Néel AFM state on the $S = 1$ quantum spin chain into an unconventional AFQ state by applying the adiabatic Floquet protocol (starting with an $\Omega = \infty$ initial state and adiabatically decreasing Ω). We chose to drive the rhombic anisotropy in Eq. (12), as it contains squares of the spin operators. Up to the time scales considered, the engineered state remains stable when the final frequency is kept fixed.

The range of amplitudes A and final frequencies Ω_f where such an AFQ state is observed is shown in the phase diagram of Fig. 6. While we are limited to relatively large Ω_f in terms of numerics, we surmise that the spin-nematic region extends to smaller Ω_f (and therefore smaller A according to Fig. 6).

In contrast to this, we find that an initial state belonging to the symmetry-protected Haldane phase is robust against such driving, as evidenced by the preserved string order parameter. Thus, while a lot of the previous interest in $S = 1$ chains was motivated by an experimental realization of Haldane physics, we find that its robustness limits the possibilities for nonequilibrium engineering. We therefore propose that conventional Néel-ordered compounds are more useful in this regard. We see that the easy-axis anisotropy is crucial in stabilizing a net quadrupole moment.

Overall, the adiabatic Floquet protocol presents a controlled approach to driven systems to manipulate and engineer valuable quantum states. Due to the adiabatic changes, we can achieve much longer numerical propagation times than in the case of sudden quenches.

From a technical perspective, we have employed MPSs in combination with the iTEBD algorithm; we have also used ED (see Appendix B) to back up our claims. Due to the adiabatic nature of the quench, a bond dimension of $\chi = 200$ is sufficient to bound the discarded weight from above. In fact, we provided analytical arguments that the drive from the Néel state can essentially be encoded with $\chi = 3$. For small discarded weights shown in Appendix B, however, we observe a fast increase of the bond dimension and thus, in principle, an uncontrolled error on this scale. This might be attributed to nongeneric features of the micromotion, though we lack a clear understanding of this issue, which is beyond the scope of this paper.

An experimental realization for the driven $S = 1$ spin chain considered here can be either using lasers with real materials [25,56,78] (cf. Fig. 1) or in cold-atom systems [91].

ACKNOWLEDGMENTS

We acknowledge support by the Niedersächsisches Vorab through the Quantum- and Nano-Metrology (QUANOMET) within the project P-1. The authors would like to thank the Publication Fund of the TU Braunschweig for financially supporting the freely accessible publication of this article.

APPENDIX A: DETAILS OF THE TIME DISCRETIZATION

To perform an adiabatic variation of the driving frequency Ω , we proceed as follows: We logarithmically discretize [92] the interval $[\Omega_f, \Omega_0]$ into $N_{\text{cycles}} + 1$ points $\{\Omega_j\}_{j=0, \dots, N_{\text{cycles}}}$, where N_{cycles} determines the total number of cycles completed by the drive in the time window $[0, t_f]$; thus, t_f is completely determined by the N_{cycles} parameter.

The adiabatic limit is realized with $N_{\text{cycles}} \rightarrow \infty$ (equivalently $t_f \rightarrow \infty$). Numerically, we fix $N_{\text{cycles}} = 300$. After a single cycle is performed with period T_j from times $[t_j, t_{j+1}] \in [0, t_f]$, we decrease the frequency by $\delta\Omega_j$ from $\Omega_j \rightarrow \Omega_j - \delta\Omega_j$, with the corresponding increment in the period $T_j \rightarrow T_j + \delta T_j$. For times $t > t_f$, we keep the frequency constant and equal to Ω_f , evolving the state to a final time $t_{\text{end}} = \alpha t_f$.

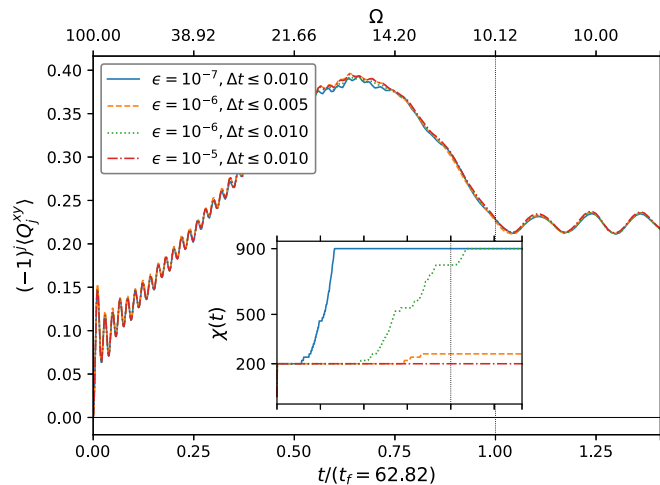


FIG. 8. The same as Fig. 5(b) with $A = 6$ but for different discarded weights ϵ and maximum Trotter steps Δt . *Inset*: The corresponding matrix-product state (MPS) bond dimension as a function of time. Horizontal axis ticks and labels correspond to those of the main panel.

APPENDIX B: NUMERICAL TESTS

In Fig. 8, we show the quadrupole polarization $(-1)^j(Q_j^{xy})$ following a quench from the Néel phase for different values of the discarded weight ϵ and maximum Trotter steps Δt [the setup is analogous to Fig. 5(b) which was obtained using $\epsilon = 10^{-5}$ and $\Delta t = 0.01$]. The corresponding bond dimension is shown in the inset. Once a maximum value of $\chi = 900$ has been reached, the bond dimension is no longer increased due to computational limitations, and the time evolution is carried out using a fixed χ . We note that the error is no longer strictly controlled in this regime.

At a maximum $\Delta t = 0.01$, the bond dimension does not increase for $\epsilon = 10^{-5}$, but it increases mildly for $\epsilon = 10^{-6}$ and rapidly for $\epsilon = 10^{-7}$, where its maximum value of $\chi = 900$ is reached quickly and the error is no longer controlled. This issue persists even if the quench is made more adiabatic ($N_{\text{cycles}} = 500$). Physical quantities, such as the quadrupole polarization, however, seem converged. It is reasonable to assume that our adiabatic protocol can be modeled accurately using a small χ (in fact, $\chi = 3$ seems sufficient, see the analytic discussion in Sec. IV B 5). A possible explanation is that the blowup of the bond dimension at small ϵ is related to features of the micromotion.

We add supportive evidence by comparing with ED data obtained system sizes of $L \leq 12$ with periodic boundary conditions. The results are shown in Fig. 9. One can see that both approaches agree qualitatively and even quantitatively unless Ω_f is small or A is large. The ED data indicate a finite steady-state value of the quadrupole polarization (or a trend in this direction as L is increased).

Finally, since time propagation using ED poses no entanglement problem, we check the robustness of the quasisteady state for very long propagation times, using $N_{\text{cycles}} = 1000$, so that $t_f \approx 190$, $t_{\text{end}} = 2.5t_f \approx 475$, and finite systems of up to $L = 10$. The result is shown in Fig. 10. We observe that the quasisteady state remains robust in this parameter range.

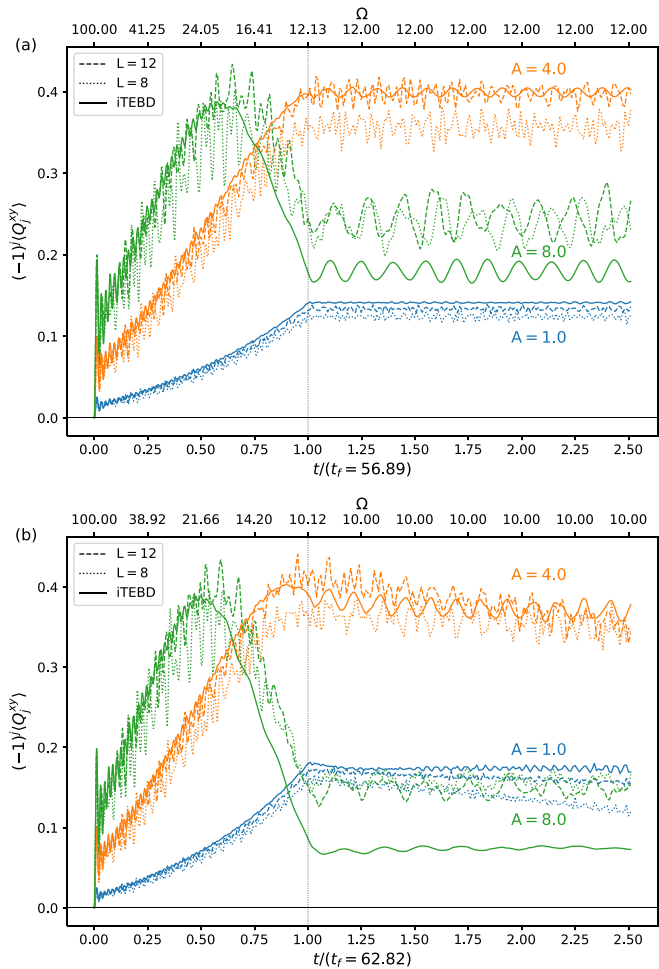


FIG. 9. Comparison of infinite time-evolving block decimation (iTEBD) and exact diagonalization (ED) results for the time evolution of the net quadrupole moment following a quench starting from the Néel phase for (a) $\Omega_f = 12.0$ and (b) $\Omega_f = 10.0$ (the latter corresponds to Figs. 5 and 8).

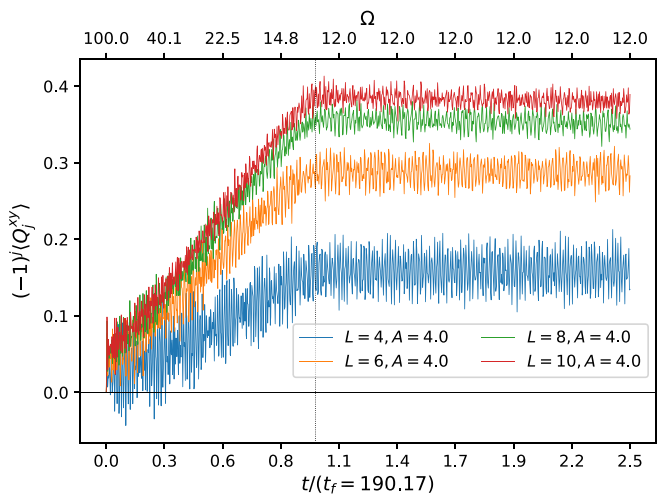


FIG. 10. Study of the stability of the quasisteady state for $A = 4$, $\Omega_f = 12$ and very long propagation times ($N_{\text{cycles}} = 1000$) using exact diagonalization in a small system of $L = 4, 6, 8, 10$.

APPENDIX C: FLOQUET HAMILTONIAN IN ADIABATIC EVOLUTION

In this section, we present general expressions for the Floquet adiabatic evolution that can be used as a starting point for methods beyond the direct time propagation used in this paper.

Given a purely periodic Hamiltonian $H(t+T) = H(t)$ with period T , the Floquet Hamiltonian H_F is formally defined by the unitary operator over a single cycle in the time interval $[t_0, t_0 + T]$:

$$U(t_0 + T, t_0) = \hat{T} \exp \left[-i \int_{t_0}^{t_0+T} ds H(s) \right] \equiv \exp(-iH_F T), \quad (\text{C1})$$

where \hat{T} is the time-ordering operator. Note that, in general, the Floquet Hamiltonian is dependent upon both t_0 and T , i.e., $H_F \equiv H_F(t_0, T)$. In most cases, determining H_F in an exact way is not possible due to the complex time ordering appearing on the right-hand side. A common approach to approximate H_F for a fixed frequency $\Omega = 2\pi/T$ is to truncate the Magnus expansion to a given order or to employ an effective Hamiltonian; however, the validity of these approaches is normally restricted to the region of high Ω values.

In the adiabatic Floquet approach described in Sec. II B, we start with the initial frequency $\Omega_0 = \infty$, where H_F is known exactly. Due to the slow decrease in Ω , H_F undergoes infinitesimal changes [and so does the unitary evolution operator in Eq. (C1)]. To determine the adiabatic variation of H_F , we look at two neighboring cycles with the drive period differing by an infinitesimal amount δT and employ in their respective intervals the definition given by Eq. (C1). This way, one does not need to solve any of the Floquet Hamiltonian problems individually, as only the difference between the series expansions of Eq. (C1) needs to be considered.

We discretize the time interval $[t_0, t_f]$ as a set of points $t_{k=0, \dots, N=f}$. The values of t_k will be called the *switching* times, representing the times where an infinitesimal variation of the driving period δT takes place. In each interval $[t_{k-1}, t_{k-1} + T_k]$, the value of the drive frequency is fixed and given by $\Omega_k = 2\pi/T_k$, and the drive function $f(t)$ satisfies

$$f(t + T_k) = f(t), \quad \forall t \in [t_{k-1}, t_{k-1} + T_k]. \quad (\text{C2})$$

We consider a time-dependent Hamiltonian of the form:

$$H(t) = H_0 + V(t), \\ V(t) = f(t) \sum_j X_j = f(t)X, \quad (\text{C3})$$

where H_0 is the time-independent part, and X_j are generic local operators. To simplify calculations, we further impose the following restriction on the drive function within each finite interval:

$$f(0) = f(T) = 0, \quad \int_{t_{k-1}}^{t_{k-1}+T_k} ds f(s) = 0, \quad \forall k. \quad (\text{C4})$$

Since the initial Hamiltonian H_0 is known, one can choose to start from an eigenstate of H_0 . In that case, it is more convenient to work in the interaction representation, where the

time evolution operator is explicitly given by

$$U(t_f, t_0) = \hat{T} \exp \left[-i \int_{t_0}^{t_f} ds \exp(iH_0 s) V(s) \exp(-iH_0 s) \right]. \quad (\text{C5})$$

On each time interval $[t_{k-1}, t_{k-1} + T_k]$, we associate a Hermitian operator $H_F^{(k)}$ defining the Floquet Hamiltonian in that interval:

$$U(t_{k-1} + T_k, t_{k-1}) \equiv \exp[-iH_F^{(k)} T_k] = U_F^{(k)}, \\ U(t_f, t_0) = \prod_{k=1}^N U_F^{(k)}. \quad (\text{C6})$$

The last identity follows from the connection property of the evolution operator. Within a given time interval of fixed period T_k , the series expansion for the unitary operator is

$$U_F^{(k)} = \sum_{n=0}^{\infty} \frac{(-i)^n}{n!} \int_{t_{k-1}}^{t_{k-1}+T_k} \prod_{j=1}^n dt_j \hat{T} [\hat{V}_k(t_j)], \quad (\text{C7})$$

where the carets indicate that the operators are in the interaction representation, i.e., $\hat{V}_k(s) = \exp(iH_0 s) V_k(s) \exp(-iH_0 s)$, and we define $V_k(s) \equiv f(s, T_k) X$ [see Eq. (C3)] for a fixed value of the period T_k . The term in brackets contains a product of the operators $\hat{V}_k(t_j)$ whose order is irrelevant due to the time-ordering operator acting over the bracket.

We consider now two adjacent unitary operators:

$$U_F^{(k)} = \exp[-iH_F^{(k)} T_k], \\ U_F^{(k+1)} = \exp[-iH_F^{(k)}(T_k + \delta T) - i\delta V_k(T_k + \delta T)], \quad (\text{C8})$$

with $\delta T \sim 0$ an infinitesimal variation of the period, and δV_k representing an infinitesimal change of the Floquet operator when a decrease in the driving frequency from Ω_k to Ω_{k+1} takes place. The first interval of the evolution is $[t_{k-1}, t_{k-1} + T_k]$, and the second is $[t_{k-1} + T_k, t_{k-1} + 2T_k + \delta T]$.

The initial form of the Floquet Hamiltonian is known in the $\Omega \rightarrow \infty$ limit:

$$H_F^{(k=0)} = H_0. \quad (\text{C9})$$

The variation with respect to the period is given by

$$\lim_{\delta T \rightarrow 0} \frac{U_F^{(k+1)} - U_F^{(k)}}{\delta T} \equiv \partial_T U_F(T). \quad (\text{C10})$$

The two neighboring terms are explicitly written in their series expansion:

$$U_F^{(k)} = \sum_{n=0}^{\infty} \frac{(-i)^n}{n!} \int_{t_{k-1}}^{t_{k-1}+T_k} \prod_{j=1}^n dt_j \hat{T} [\hat{V}_k(t_j)], \\ U_F^{(k+1)} = \sum_{n=0}^{\infty} \frac{(-i)^n}{n!} \int_{t_{k-1}+T_k}^{t_{k-1}+2T_k+\delta T} \prod_{j=1}^n dt_j \hat{T} [\hat{V}_{k+1}(t_j)]. \quad (\text{C11})$$

By changing the variables of integration in the $U_F^{(k+1)}$ to $\tilde{t}_n = t_n - T_k$, we obtain two different contributions when subtract-

ing both series $\Delta U_F^{(k)} = U_F^{(k+1)} - U_F^{(k)}$:

$$\Delta U_F^{(k)} = \sum_{n=1}^{\infty} \frac{(-i)^n}{n!} \int_{t_{k-1}}^{t_{k-1}+T_k} \prod_{j=1}^n dt_j \hat{T}[\Delta \hat{O}_k(\{t_j\})] + \sum_{n=1}^{\infty} \frac{(-i)^n}{n!} \int_{t_{k-1}+T_k}^{t_{k-1}+T_k+\delta T} \prod_{j=1}^n dt_j \hat{T}[\hat{O}_{k+1}(\{t_j\})], \tag{C12}$$

where we have defined

$$\hat{O}_k(\{t_j\}) = \hat{V}_k(t_1) \dots \hat{V}_k(t_n), \tag{C13}$$

$$\Delta \hat{O}_k(\{t_j\}) = \hat{O}_{k+1}(\{t_j\}) - \hat{O}_k(\{t_j\}).$$

Note that all summed up terms start at $n = 1$ since the identities appearing on the right-hand side have canceled out. For the $k + 1$ term, we make use of the following expansion:

$$\hat{O}_{k+1}(\{t_j\}) \approx \underbrace{\hat{V}_k(t_1) \dots \hat{V}_k(t_n)}_{=\hat{O}_k(\{t_j\})} + \delta T \sum_{j=1}^n \frac{\partial \hat{V}_k(t_j)}{\partial T} \prod_{l \neq j} \hat{V}_k(t_l). \tag{C14}$$

We stress that the order of products inside the brackets is irrelevant due to the action of the time-ordering operator. The second term in the right-hand side of Eq. (C12) is identically zero when Eq. (C4) is satisfied over the infinitesimal interval of integration. For the first series, the term in brackets at a given order n is given by

$$(\delta T) \hat{T} \left\{ \sum_{j=1}^n \frac{1}{f(t_j, T_k)} \left[\frac{\partial f(t_j, T)}{\partial T} \right] \Big|_{T=T_k} \hat{O}_k(\{t_j\}) \right\}. \tag{C15}$$

Due to the time ordering, each summand will give exactly the same contribution to the propagator. Then we can select one of

the intermediate times (say t_1), sweep it around the full string of operators, and write

$$\alpha_n \int_a^b dt_1 w(t_1, T_k) \hat{V}_k(t_1) \int_a^b dt_2 \dots \int_a^b dt_n \hat{T} \hat{O}_k(\{t_j\}), \tag{C16}$$

$$\alpha_n = \frac{(-i)^n}{n!} (\delta T)^n,$$

where we have abbreviated $a = t_{k-1}$ and $b = t_{k-1} + T_k$, and defined

$$w(t_1, T_k) = \left[\frac{\partial f(t_1, T)}{\partial T} \right] \Big|_{T=T_k} \frac{1}{f(t_1, T_k)}. \tag{C17}$$

We can arrange t_1 a total of n times, with the remaining $n - 1$ operators still subjected to time ordering. Proceeding to all orders, Eq. (C12) becomes

$$\Delta U_F^{(k)} \approx -i \delta T \int_a^b dt_1 w(t_1, T_k) \hat{V}_k(t_1, T_k) U_F^k. \tag{C18}$$

Equation (C18) gives a differential equation for the Floquet unitary operator. The initial condition is given by

$$U_F(T = 0) = \lim_{T \rightarrow 0} \exp(-iH_0 T) = 1. \tag{C19}$$

The corresponding Floquet Hamiltonian is then identified by the relation:

$$U_F(T) = \exp[-iH_F(T)T],$$

$$H_F(T) = \frac{1}{T} \int_{t_0(T)}^{t_0(T)+T} ds \exp(iH_0 s) V(s, T) \exp(-iH_0 s). \tag{C20}$$

Note that the exact form of increments in the period T is what determines the functional form of the switching times $t_0(T)$.

[1] L. Mazza, D. Rossini, M. Endres, and R. Fazio, Out-of-equilibrium dynamics and thermalization of string order, *Phys. Rev. B* **90**, 020301(R) (2014).

[2] M. Calvanese Strinati, L. Mazza, M. Endres, D. Rossini, and R. Fazio, Destruction of string order after a quantum quench, *Phys. Rev. B* **94**, 024302 (2016).

[3] M. Moeckel and S. Kehrein, Interaction Quench in the Hubbard Model, *Phys. Rev. Lett.* **100**, 175702 (2008).

[4] A. Sen, D. Sen, and K. Sengupta, Analytic approaches to periodically driven closed quantum systems: Methods and applications, *J. Phys.: Condens. Matter* **33**, 443003 (2021).

[5] M. Bukov, L. D'Alessio, and A. Polkovnikov, Universal high-frequency behavior of periodically driven systems: From dynamical stabilization to Floquet engineering, *Adv. Phys.* **64**, 139 (2015).

[6] D. A. Abanin, W. De Roeck, and F. Huveneers, Exponentially Slow Heating in Periodically Driven Many-Body Systems, *Phys. Rev. Lett.* **115**, 256803 (2015).

[7] T. Oka and S. Kitamura, Floquet engineering of quantum materials, *Annu. Rev. Condens. Matter Phys.* **10**, 387 (2019).

[8] C. Weitenberg and J. Simonet, Tailoring quantum gases by floquet engineering, *Nat. Phys.* **17**, 1342 (2021).

[9] A. de la Torre, D. M. Kennes, M. Claassen, S. Gerber, J. W. McIver, and M. A. Sentef, Colloquium: Nonthermal pathways to ultrafast control in quantum materials, *Rev. Mod. Phys.* **93**, 041002 (2021).

[10] D. M. Kennes, A. de la Torre, A. Ron, D. Hsieh, and A. J. Millis, Floquet Engineering in Quantum Chains, *Phys. Rev. Lett.* **120**, 127601 (2018).

[11] T. Oka and H. Aoki, Photovoltaic Hall effect in graphene, *Phys. Rev. B* **79**, 081406(R) (2009).

[12] T. Kitagawa, E. Berg, M. Rudner, and E. Demler, Topological characterization of periodically driven quantum systems, *Phys. Rev. B* **82**, 235114 (2010).

[13] N. H. Lindner, G. Refael, and V. Galitski, Floquet topological insulator in semiconductor quantum wells, *Nat. Phys.* **7**, 490 (2011).

[14] M. S. Rudner, N. H. Lindner, E. Berg, and M. Levin, Anomalous Edge States and the Bulk-Edge Correspondence for Periodically Driven Two-Dimensional Systems, *Phys. Rev. X* **3**, 031005 (2013).

- [15] D. Fausti, R. I. Tobey, N. Dean, S. Kaiser, A. Dienst, M. C. Hoffmann, S. Pyon, T. Takayama, H. Takagi, and A. Cavalleri, Light-induced superconductivity in a stripe-ordered cuprate, *Science* **331**, 189 (2011).
- [16] M. Mitrano, A. Cantaluppi, D. Nicoletti, S. Kaiser, A. Perucchi, S. Lupi, P. Di Pietro, D. Pontiroli, M. Riccò, S. R. Clark *et al.*, Possible light-induced superconductivity in K_3C_{60} at high temperature, *Nature (London)* **530**, 461 (2016).
- [17] M. Babadi, M. Knap, I. Martin, G. Refael, and E. Demler, Theory of parametrically amplified electron-phonon superconductivity, *Phys. Rev. B* **96**, 014512 (2017).
- [18] A. Sheikhan and C. Kollath, Dynamically enhanced unconventional superconducting correlations in a Hubbard ladder, *Phys. Rev. B* **102**, 035163 (2020).
- [19] S. Kitamura and H. Aoki, η -pairing superfluid in periodically-driven fermionic Hubbard model with strong attraction, *Phys. Rev. B* **94**, 174503 (2016).
- [20] T. Kaneko, T. Shirakawa, S. Sorella, and S. Yunoki, Photoinduced η Pairing in the Hubbard Model, *Phys. Rev. Lett.* **122**, 077002 (2019).
- [21] F. Peronaci, O. Parcollet, and M. Schirò, Enhancement of local pairing correlations in periodically driven Mott insulators, *Phys. Rev. B* **101**, 161101(R) (2020).
- [22] K. Takasan, M. Nakagawa, and N. Kawakami, Laser-irradiated Kondo insulators: Controlling the Kondo effect and topological phases, *Phys. Rev. B* **96**, 115120 (2017).
- [23] J. H. Mentink, K. Balzer, and M. Eckstein, Ultrafast and reversible control of the exchange interaction in Mott insulators, *Nat. Commun.* **6**, 6708 (2015).
- [24] M. Sato, S. Takayoshi, and T. Oka, Laser-Driven Multiferroics and Ultrafast Spin Current Generation, *Phys. Rev. Lett.* **117**, 147202 (2016).
- [25] S. Takayoshi, H. Aoki, and T. Oka, Magnetization and phase transition induced by circularly polarized laser in quantum magnets, *Phys. Rev. B* **90**, 085150 (2014).
- [26] K. S. C. Decker, C. Karrasch, J. Eisert, and D. M. Kennes, Floquet Engineering Topological Many-Body Localized Systems, *Phys. Rev. Lett.* **124**, 190601 (2020).
- [27] P. Weinberg, M. Bukov, L. D'Alessio, A. Polkovnikov, S. Vajna, and M. Kolodrubetz, Adiabatic perturbation theory and geometry of periodically-driven systems, *Phys. Rep.* **688**, 1 (2017).
- [28] S. Guérin and H. Jauslin, Control of quantum dynamics by laser pulses: Adiabatic Floquet theory, in *Advances in Chemical Physics*, edited by I. Prigogine and S. A. Rice (Wiley, Hoboken, 2003), Vol. 125, pp. 147–267.
- [29] A. Russomanno and E. G. D. Torre, Kibble-Zurek scaling in periodically driven quantum systems, *Europhys. Lett.* **115**, 30006 (2016).
- [30] A. Russomanno, B.-E. Friedman, and E. G. Dalla Torre, Spin and topological order in a periodically driven spin chain, *Phys. Rev. B* **96**, 045422 (2017).
- [31] U. Schollwöck, The density-matrix renormalization group in the age of matrix product states, *Ann. Phys.* **326**, 96 (2011).
- [32] P. Calabrese and J. Cardy, Evolution of entanglement entropy in one-dimensional systems, *J. Stat. Mech.: Theory Exp.* (2005) P04010.
- [33] The correspondence arises from the comparison of quantum spin-spin correlations to classical density-density correlations, which are long-ranged in a solid (corresponding to a ferromagnet) and exponentially decaying in a liquid (corresponding to a disordered spin liquid). In a nematic liquid crystal, they are disordered like in a liquid, but rodlike molecules order along a preferred axis.
- [34] T. Sakai and M. Takahashi, Effect of the Haldane gap on quasi-one-dimensional systems, *Phys. Rev. B* **42**, 4537 (1990).
- [35] M. Tsukano and K. Nomura, Berezinskii-Kosterlitz-Thouless transition of spin-1 XXZ chains in a staggered magnetic field, *J. Phys. Soc. Jpn.* **67**, 302 (1998).
- [36] K. Wierschem and P. Sengupta, Characterizing the Haldane phase in quasi-one-dimensional spin-1 Heisenberg antiferromagnets, *Mod. Phys. Lett. B* **28**, 1430017 (2014).
- [37] A. K. Bera, B. Lake, A. T. M. N. Islam, O. Janson, H. Rosner, A. Schneidewind, J. T. Park, E. Wheeler, and S. Zander, Consequences of critical interchain couplings and anisotropy on a Haldane chain, *Phys. Rev. B* **91**, 144414 (2015).
- [38] W. J. L. Buyers, R. M. Morra, R. L. Armstrong, M. J. Hogan, P. Gerlach, and K. Hirakawa, Experimental Evidence for the Haldane Gap in a Spin-1 Nearly Isotropic, Antiferromagnetic Chain, *Phys. Rev. Lett.* **56**, 371 (1986).
- [39] R. M. Morra, W. J. L. Buyers, R. L. Armstrong, and K. Hirakawa, Spin dynamics and the Haldane gap in the spin-1 quasi-one-dimensional antiferromagnet $CsNiCl_3$, *Phys. Rev. B* **38**, 543 (1988).
- [40] H. Mutka, C. Payen, P. Molinié, J. L. Soubeyroux, P. Colombet, and A. D. Taylor, Dynamic Structure Factor $[S(Q,\omega)]$ of the $S = 1$ Quasi-One-Dimensional Heisenberg Antiferromagnet: Neutron-Scattering Study on $AgVP_2$, *Phys. Rev. Lett.* **67**, 497 (1991).
- [41] T. Asano, Y. Ajiro, M. Mekata, H. Yamazaki, N. Hosoito, T. Shinjo, and H. Kikuchi, Single crystal susceptibility of the $S = 1$ one-dimensional Heisenberg antiferromagnet $AgVP_2S_6$, *Solid State Commun.* **90**, 125 (1994).
- [42] M. Takigawa, T. Asano, Y. Ajiro, and M. Mekata, Static properties of the $S = 1$ one-dimensional antiferromagnet $AgVP_2S_6$, *Phys. Rev. B* **52**, R13087(R) (1995).
- [43] M. Takigawa, T. Asano, Y. Ajiro, M. Mekata, and Y. J. Uemura, Dynamics in the $S = 1$ One-Dimensional Antiferromagnet $AgVP_2S_6$ via ^{31}P and ^{51}V NMR, *Phys. Rev. Lett.* **76**, 2173 (1996).
- [44] Z. Honda, K. Katsumata, Y. Nishiyama, and I. Harada, Field-induced long-range ordering in an $s = 1$ quasi-one-dimensional Heisenberg antiferromagnet, *Phys. Rev. B* **63**, 064420 (2001).
- [45] E. Čížmár, M. Ozerov, O. Ignatchik, T. P. Papageorgiou, J. Wosnitza, S. A. Zvyagin, J. Krzystek, Z. Zhou, C. P. Landee, B. R. Landry *et al.*, Magnetic properties of the Haldane-gap material $[Ni(C_2H_8N_2)_2NO_2](BF_4)$, *New J. Phys.* **10**, 033008 (2008).
- [46] J. P. Renard, M. Verdaguer, L. P. Regnault, W. A. C. Erkelens, J. Rossat-Mignod, and W. G. Stirling, Presumption for a quantum energy gap in the quasi-one-dimensional $S = 1$ heisenberg antiferromagnet $Ni(C_2H_8N_2)_2NO_2(ClO_4)$, *Europhys. Lett.* **3**, 945 (1987).
- [47] L. P. Regnault, I. Zaliznyak, J. P. Renard, and C. Vettier, Inelastic-neutron-scattering study of the spin dynamics in the Haldane-gap system $Ni(C_2H_8N_2)_2NO_2ClO_4$, *Phys. Rev. B* **50**, 9174 (1994).

- [48] I. A. Zaliznyak, D. C. Dender, C. Broholm, and D. H. Reich, Tuning the spin Hamiltonian of $\text{Ni}(\text{C}_2\text{H}_8\text{N}_2)_2\text{NO}_2\text{ClO}_4$ by external pressure: A neutron-scattering study, *Phys. Rev. B* **57**, 5200 (1998).
- [49] Y. Uchiyama, Y. Sasago, I. Tsukada, K. Uchinokura, A. Zheludev, T. Hayashi, N. Miura, and P. Böni, Spin-Vacancy-Induced Long-Range Order in a New Haldane-Gap Antiferromagnet, *Phys. Rev. Lett.* **83**, 632 (1999).
- [50] A. Zheludev, T. Masuda, I. Tsukada, Y. Uchiyama, K. Uchinokura, P. Böni, and S.-H. Lee, Magnetic excitations in coupled Haldane spin chains near the quantum critical point, *Phys. Rev. B* **62**, 8921 (2000).
- [51] B. Pahari, K. Ghoshray, R. Sarkar, B. Bandyopadhyay, and A. Ghoshray, NMR study of ^{51}V in quasi-one-dimensional integer spin chain compound $\text{SrNi}_2\text{V}_2\text{O}_8$, *Phys. Rev. B* **73**, 012407 (2006).
- [52] A. K. Bera, B. Lake, A. T. M. N. Islam, B. Klemke, E. Faulhaber, and J. M. Law, Field-induced magnetic ordering and single-ion anisotropy in the quasi-one-dimensional Haldane chain compound $\text{SrNi}_2\text{V}_2\text{O}_8$: A single-crystal investigation, *Phys. Rev. B* **87**, 224423 (2013).
- [53] V. Gadet, M. Verdaguer, V. Briois, A. Gleizes, J. P. Renard, P. Beauvillain, C. Chappert, T. Goto, K. Le Dang, and P. Veillet, Structural and magnetic properties of $(\text{CH}_3)_4\text{NNi}(\text{NO}_2)_3$: A Haldane-gap system, *Phys. Rev. B* **44**, 705 (1991).
- [54] J. Darriet and L. Regnault, The compound Y_2BaNiO_5 : A new example of a haldane gap in a $S = 1$ magnetic chain, *Solid State Commun.* **86**, 409 (1993).
- [55] G. Xu, J. F. DiTusa, T. Ito, K. Oka, H. Takagi, C. Broholm, and G. Aeppli, Y_2BaNiO_5 : A nearly ideal realization of the $S = 1$ Heisenberg chain with antiferromagnetic interactions, *Phys. Rev. B* **54**, R6827(R) (1996).
- [56] V. Gnezdilov, V. Kurnosov, Y. Pashkevich, A. K. Bera, A. T. M. N. Islam, B. Lake, B. Lobbenmeier, D. Wulferding, and P. Lemmens, Non-Abelian statistics in light-scattering processes across interacting Haldane chains, *Phys. Rev. B* **104**, 165118 (2021).
- [57] M. Orendáč, A. Orendáčová, J. Cernáč, A. Feher, P. J. C. Signore, M. W. Meisel, S. Merah, and M. Verdaguer, Thermodynamic and magnetic properties of the $S = 1$ Heisenberg chain $\text{Ni}(\text{C}_2\text{H}_8\text{N}_2)_2\text{Ni}(\text{CN})_4$: Experiments and theory, *Phys. Rev. B* **52**, 3435 (1995).
- [58] F. D. M. Haldane, Nonlinear Field Theory of Large-Spin Heisenberg Antiferromagnets: Semiclassically Quantized Solitons of the One-Dimensional Easy-Axis Néel State, *Phys. Rev. Lett.* **50**, 1153 (1983).
- [59] F. Haldane, Continuum dynamics of the 1-D Heisenberg antiferromagnet: Identification with the $O(3)$ nonlinear sigma model, *Phys. Lett. A* **93**, 464 (1983).
- [60] I. Affleck, T. Kennedy, E. H. Lieb, and H. Tasaki, Rigorous results on valence-bond ground states in antiferromagnets, in *Condensed Matter Physics and Exactly Soluble Models*, edited by B. Nachtergaele, J. P. Solovej, and J. Yngvason (Springer, Berlin, Heidelberg, 2004), pp. 249–252.
- [61] I. Affleck, T. Kennedy, E. H. Lieb, and H. Tasaki, Valence bond ground states in isotropic quantum antiferromagnets, *Commun. Math. Phys.* **115**, 477 (1988).
- [62] F. Pollmann, A. M. Turner, E. Berg, and M. Oshikawa, Entanglement spectrum of a topological phase in one dimension, *Phys. Rev. B* **81**, 064439 (2010).
- [63] F. Pollmann, E. Berg, A. M. Turner, and M. Oshikawa, Symmetry protection of topological phases in one-dimensional quantum spin systems, *Phys. Rev. B* **85**, 075125 (2012).
- [64] F. Pollmann and A. M. Turner, Detection of symmetry-protected topological phases in one dimension, *Phys. Rev. B* **86**, 125441 (2012).
- [65] M. den Nijs and K. Rommelse, Preroughening transitions in crystal surfaces and valence-bond phases in quantum spin chains, *Phys. Rev. B* **40**, 4709 (1989).
- [66] T. Kennedy and H. Tasaki, Hidden symmetry breaking and the Haldane phase in $S = 1$ quantum spin chains, *Commun. Math. Phys.* **147**, 431 (1992).
- [67] M. Oshikawa, Hidden $Z_2 * Z_2$ symmetry in quantum spin chains with arbitrary integer spin, *J. Phys.: Condens. Matter* **4**, 7469 (1992).
- [68] M. Blume and Y. Hsieh, Biquadratic exchange and quadrupolar ordering, *J. Appl. Phys.* **40**, 1249 (1969).
- [69] M. N. Barber and M. T. Batchelor, Spectrum of the biquadratic spin-1 antiferromagnetic chain, *Phys. Rev. B* **40**, 4621 (1989).
- [70] A. Läuchli, G. Schmid, and S. Trebst, Spin nematics correlations in bilinear-biquadratic $S = 1$ spin chains, *Phys. Rev. B* **74**, 144426 (2006).
- [71] A. V. Chubukov, Spontaneous dimerization in quantum-spin chains, *Phys. Rev. B* **43**, 3337 (1991).
- [72] K. Buchta, G. Fáth, O. Legeza, and J. Sólyom, Probable absence of a quadrupolar spin-nematic phase in the bilinear-biquadratic spin-1 chain, *Phys. Rev. B* **72**, 054433 (2005).
- [73] I. Niesen and P. Corboz, A tensor network study of the complete ground state phase diagram of the spin-1 bilinear-biquadratic Heisenberg model on the square lattice, *SciPost Phys.* **3**, 030 (2017).
- [74] K. Harada and N. Kawashima, Quadrupolar order in isotropic Heisenberg models with biquadratic interaction, *Phys. Rev. B* **65**, 052403 (2002).
- [75] Y. C. Tzeng, H. Onishi, T. Okubo, and Y. J. Kao, Quantum phase transitions driven by rhombic-type single-ion anisotropy in the $S = 1$ Haldane chain, *Phys. Rev. B* **96**, 060404(R) (2017).
- [76] M. T. Batchelor, X.-W. Guan, and N. Oelkers, Thermal and magnetic properties of spin-1 magnetic chain compounds with large single-ion and in-plane anisotropies, *Phys. Rev. B* **70**, 184408 (2004).
- [77] A. Abragam and B. Bleaney, *Electron Paramagnetic Resonance of Transition Ions* (Oxford University Press, Oxford, 2012).
- [78] U. F. P. Seifert, M. Ye, and L. Balents, Ultrafast optical excitation of magnetic dynamics in van der Waals magnets: Coherent magnons and BKT dynamics in NiPS_3 , *Phys. Rev. B* **105**, 155138 (2022).
- [79] M. Kitagawa and M. Ueda, Squeezed spin states, *Phys. Rev. A* **47**, 5138 (1993).
- [80] J. Ma, X. Wang, C. Sun, and F. Nori, Quantum spin squeezing, *Phys. Rep.* **509**, 89 (2011).
- [81] M. E. Zhitomirsky and H. Tsunetsugu, Magnon pairing in quantum spin nematic, *Europhys. Lett.* **92**, 37001 (2010).
- [82] A. Orlova, E. L. Green, J. M. Law, D. I. Gorbunov, G. Chanda, S. Krämer, M. Horvatić, R. K. Kremer, J. Wosnitzer, and G. L. J. A. Rikken, Nuclear Magnetic Resonance Signature of the Spin-Nematic Phase in LiCuVO_4 at High Magnetic Fields, *Phys. Rev. Lett.* **118**, 247201 (2017).
- [83] L. Svistov, T. Fujita, H. Yamaguchi, S. Kimura, K. Omura, A. Prokofiev, A. I. Smirnov, Z. Honda, and M. Hagiwara, New

- high magnetic field phase of the frustrated $S = \frac{1}{2}$ chain compound LiCuVO_4 , [JETP Lett. **93**, 21 \(2011\)](#).
- [84] J. Lou, T. Xiang, and Z. Su, Thermodynamics of the Bilinear-Biquadratic Spin-One Heisenberg Chain, [Phys. Rev. Lett. **85**, 2380 \(2000\)](#).
- [85] P. Millet, F. Mila, F. C. Zhang, M. Mambrini, A. B. Van Oosten, V. A. Pashchenko, A. Sulpice, and A. Stepanov, Biquadratic Interactions and Spin-Peierls Transition in the Spin-1 Chain LiVGe_2O_6 , [Phys. Rev. Lett. **83**, 4176 \(1999\)](#).
- [86] F. Mila and F.-C. Zhang, On the origin of biquadratic exchange in spin 1 chains, [Eur. Phys. J. B **16**, 7 \(2000\)](#).
- [87] S. Paeckel, T. Köhler, A. Swoboda, S. R. Manmana, U. Schollwöck, and C. Hubig, Time-evolution methods for matrix-product states, [Ann. Phys. **411**, 167998 \(2019\)](#).
- [88] G. Vidal, Classical Simulation of Infinite-Size Quantum Lattice Systems in One Spatial Dimension, [Phys. Rev. Lett. **98**, 070201 \(2007\)](#).
- [89] V. Zauner-Stauber, L. Vanderstraeten, M. T. Fishman, F. Verstraete, and J. Haegeman, Variational optimization algorithms for uniform matrix product states, [Phys. Rev. B **97**, 045145 \(2018\)](#).
- [90] A. H. Abdeldaim, D. I. Badrtdinov, A. S. Gibbs, P. Manuel, H. C. Walker, M. D. Le, C. H. Wu, D. Wardecki, S.-G. Eriksson, Y. O. Kvashnin *et al.*, Large easy-axis anisotropy in the one-dimensional magnet $\text{BaMo}(\text{PO}_4)_2$, [Phys. Rev. B **100**, 214427 \(2019\)](#).
- [91] C. Senko, P. Richerme, J. Smith, A. Lee, I. Cohen, A. Retzker, and C. Monroe, Realization of a Quantum Integer-Spin Chain with Controllable Interactions, [Phys. Rev. X **5**, 021026 \(2015\)](#).
- [92] The choice of a logarithmically spaced grid for the interval $[\Omega_f, \Omega_0]$ is just for computational purposes, favoring smaller period increments as we approach t_f . In a purely adiabatic process, such a discretization choice should be irrelevant.